# Skeletal dosimetry in the MAX06 and the FAX06 phantoms for external exposure to photons based on vertebral 3D-microCT images

**R Kramer [1], H J Khoury [1], J W Vieira [2,3] and I Kawrakow [4]**

[1] Departamento de Energia Nuclear, Universidade Federal de Pernambuco, Av. Prof. Luiz Freire 1000, Cidade Universitária, CEP 50740-540, Recife, PE, Brazil

[2] Centro Federal de Educação Tecnológica de Pernambuco, Recife, PE, Brazil

[3] Escola Politécnica, UPE, Recife, PE, Brazil

[4] Ionizing Radiation Standards, National Research Council of Canada, Ottawa, Canada

E-mail: rkramer@uol.com.br

Statement of provenance:
'This is an author-created, un-copyedited version of an article accepted for publication in Physics in Medicine and Biology. IOP Publishing Ltd is not responsible for any errors or omissions in this version of the manuscript or any version derived from it. The definitive publisher authenticated version is available at doi:10.1088/0031-9155/51/24/001. '

**ABSTRACT**

3D-microCT images of vertebral bodies from three different individuals have been segmented into trabecular bone, bone marrow and bone surface cells (BSC), and then introduced into the spongiosa voxels of the MAX06 and the FAX06 phantoms, in order to calculate the equivalent dose to the red bone marrow (RBM) and the BSC in the marrow cavities of trabecular bone with the EGSnrc Monte Carlo code from whole body exposure to external photon radiation. The MAX06 and the FAX06 phantoms consist of ca. 150 million 1.2mm cubic voxels each, a part of which are spongiosa voxels surrounded by cortical bone. In order to use the segmented 3D-microCT images for skeletal dosimetry, spongiosa voxels in the MAX06 and the FAX06 phantom were replaced at run-time by so-called micro matrices representing segmented trabecular bone, marrow and BSC in 17.65, 30 and 60 micron cubic voxels.

The 3D-microCT image-based RBM and BSC equivalent doses for external exposure to photons presented here for the first time for complete human skeletons are in agreement with the results calculated with the three correction factor (3CF) method and the fluence-to-dose response (FDR) functions for the same phantoms taking into account the conceptual differences between the different methods. Additionally the microCT image-based results have been compared with corresponding data from earlier studies for other human phantoms.

## 1. Introduction

### 1.1 The skeletal tissues at risk

According to the concept of effective dose (ICRP 1991), apart from other organs the equivalent dose has to be determined in two different skeletal soft tissues:

a) in the haematopietic stem cells of the marrow, called "red bone marrow" (RBM), and

b) in the osteogenic cells on the endosteal surfaces , called "bone surface cells" (BSC).

Both soft tissues are located in the irregularily shaped marrow cavities of trabecular bone with diameters ranging from 50 to 2000 micron (Spiers 1969). “Trabecular bone plus its supported soft tissue is sometimes also referred to as spongiosa” (ICRP 1995). The BSC, actually considered to have a thickness of 10 micron (ICRP 1979), cover the surfaces of trabecular bone, while the RBM occupies a part of the marrow volume given by the cellularity factor (ICRP 1995). In the future, however, the International Commission on Radiological Protection (ICRP) intends to recommend 50 micron for the thickness of the BSC (Eckerman 2006).

### 1.2 A short review of the history of skeletal dosimetry

A comprehensive review of the history of skeletal dosimetry would be a paper in its own rights. Therefore the following review will highlight especially contributions relevant to the concepts and the methods used in this study.

The history of skeletal dosimetry is very much connected to the name of F.W.Spiers. Spiers and his co-workers at the University of Leeds in England can be considered the most important contributors to the developement of skeletal dosimetry from its beginning in the early 50ies until the late 80ies of the last century. Conversion factors for marrow in trabecular bone from exposure to X-rays (Spiers 1963, 1969, King and Spiers 1985), the measurement of chord-length distributions in trabecular bone (Beddoe et al 1976), and the calculation of skeletal dose factors for incorporated radionuclides (Spiers 1974, Spiers et al 1978 a,b, Spiers et al 1981, Spiers 1988, Whitwell and Spiers 1976, Beddoe et al 1979) can be considered to be fundamental contributions to skeletal dosimetry, and many of them became the data base for research made in scientific laboratories all over the world.

Based on the work of the group at the University of Leeds, another important center for skeletal dosimetry was developed at the Oak Ridge National Laboratory (ORNL) by K.Eckerman in connection with the developement of the MIRD5 phantom series (Eckerman and Stabin 2000, Stabin et al 2002). With respect to the investigation presented here, especially the photon fluence-to-dose response (FDR) functions for RBM and BSC have to be mentioned (Cristy and Eckerman 1987), which are based on the chord-length distributions measured by Darley (1968), Whitwell (1973) and Beddoe et al (1976).

Application of the conversion factors for marrow in trabecular bone from external exposure to X rays (Spiers 1963) has initiated the developement of skeletal dosimetry at the National Research Center for Environment and Health in Munich in Germany. Based on a proposal by Rosenstein (1976), Kramer (1979) developed an algorithm to be applied to the MIRD5-type phantoms ADAM and EVA (Kramer et al 1982) for external photon radiation, which used rad/Roentgen conversion factors for marrow in five different bones of the human skeleton published by Spiers (1963). These so-called “Spiers factors”, or later “King-Spiers” factors (King and Spiers 1985), have also been integrated into the CT number method, developed by Zankl and Wittmann (2001), which for the first time applied a heterogeneous tissue distribution to the skeleton of a phantom.

While for about four decades the University of Leeds was the center of skeletal dosimetry, today the most advanced methods in this area come from the University of Florida. W.Bolch and his co-workers from the Nuclear and Radiological Engineering Department succeeded to segment trabecular bone and marrow in microCT and NMR images of the spongiosa of human bone samples, and to subsequently connect these segmented images to a Monte Carlo (MC) radiation transport code for the purposes of skeletal dosimetry (Bolch et al 2002, Bouchet et al 1999, Jokisch et al 2001, Patton et al 2002a,b, Rajon et al 2002, Shah et al 2003, Shah et al 2005a,b,c,d). Spongiosa in the human skeleton is usually surrounded by cortical bone. Therefore the group at the University of Florida developed a special MC transport code, called PIRT (paired-image radiation transport), which transports the particles through a “macro” matrix with a voxel size of some hundred micron, representing spongiosa, cortical bone and surrounding soft tissues, and at the same time through a “micro” matrix with cubic voxel sizes down to 30 micron, representing the micro structure of spongiosa with segmented volumes of marrow and trabecular bone. So far this new method has mainly been applied to nuclear medicine applications and only to isolated bone samples, but so far not to a complete skeleton embedded in a human body.

## 1.3 Skeletal dosimetry for exposure to photons

### 1.3.1 The three correction factor (3CF) method

The 3CF method for the calculation of equivalent dose to the RBM in the ADAM and in the EVA phantoms (Kramer et al 1982) for incident photon energies up to 200 keV was developed by Kramer (1979) following a proposal by Rosenstein (1976). The composition of the skeleton has to be a homogeneous mixture of bone and marrow. The 3CF method applies three different correction factors to the photon energy deposited in the homogeneous skeletal mixture:

a) RBM mass fractions,
b) ratios between the mass energy-absorption coefficients (MEAC) of RBM and the skeletal mixture, and
c) the King-Spiers (KS) factors (King and Spiers 1985), which represent the percentage excess RBM equivalent dose due to the flux of photo-electrons released in trabecular bone entering the marrow cavities.

King and Spiers measured photo-electron enhancement of absorbed dose in the marrow cavities with LiF powder for 3 specimens of vertebral spongiosa in a completely reconstructed vertebral body. The percentage excess doses per specimen were then combined with theoretically determined bone-specific dose factors from Whitwell and Spiers (1976) in order to get bone-specific photo-electron excess percentages in RBM as a function of the photon energy incident on the surface of the corresponding bone. The KS factors have been determined for skeletal dosimetry calculations below 200 keV which do not perform secondary charged particle transport. Therefore one has to do the calculation with kerma approximation, and when applying the KS factors one has to use the energy the photon has before entering the bone.
The study by King and Spiers does not provide similar data for the calculation of the equivalent dose to the BSC. Therefore, when the 3CF method is used to calculate the equivalent dose to the RBM, usually the average equivalent dose to the skeletal mixture is taken as a conservative estimate for the equivalent dose to the BSC. The 3CF method will be used in this study for comparison with the 3D-microCT image-based method.

### 1.3.2 Fluence-to-dose response (FDR) functions

Cristy and Eckerman (1987) developed bone-specific FDR (fluence-to-dose response) functions for photons, which relate the equivalent dose to the RBM and to the BSC to the photon fluence in a homogeneous skeleton. The FDR functions have been determined based on the interaction probabilities for photoelectric effect, Compton scattering, or pair production in trabecular bone and marrow, on the energy spectrum of the secondary particles liberated from these processes, and on energy-dependent absorbed fractions in the RBM and the BSC from secondary electrons released in trabecular bone or marrow sampled from the chord-length distributions published by Darley (1968), Whitwell (1973) and Beddoe et al (1976) for a 44-year old male. The equivalent dose to the BSC was taken as the average of the contributions from trabecular and cortical bone surfaces for a thickness of 10 micron.
The FDR functions have been developed for kerma approximation, because their purpose is to replace secondary electron transport in the micro structure of spongiosa. This study will use the FDR functions from Cristy and Eckerman for comparison with the 3D-microCT image-based method.

### 1.3.3. The CT number (CTN) method

The CTN method, developed by Zankl and Wittmann (2001), and as adopted by Kramer et al (2003, 2004a) for the MAX and the FAX phantoms, distributes three different tissues among the skeletal voxels temporarily at runtime of the MC calculation. The method uses the CT numbers (= grey values)

of the skeletal pixels from the original CT images of the patient to determine whether a skeletal voxel is cortical bone, spongiosa or marrow, thereby creating a heterogeneous tissue distribution among the skeletal voxels.
Compared to dosimetric methods which use a homogeneous skeletal mixture in all parts of the skeleton, the CTN method represents progress because it introduces the layer of cortical bone around the spongiosa voxels which skeletons usually have. However, the spongiosa voxels are still considered to be a homogeneous mixture of trabecular bone and marrow, which requires the use of the 3CF method for the energy deposited in these voxels, and, depending on the voxel resolution of the human phantom used, all or many marrow voxels are ficticious.
The width of trabecular cavities ranges from 50 to 2000 micron (Spiers 1969), while, for example, the size of the cubic voxels of the MAX/FAX phantoms is 3600 micron. However, it is not possible to segment an object with a voxel resolution which is larger than the object to be segmented. Marrow voxels of 3.6mm x 3.6mm x 3.6mm created by the CTN method in the MAX/FAX phantoms do not exist in a real human skeleton. There exist human phantoms with smaller voxel sizes, for example the MAX06 and the FAX06 phantoms which have 1.2 mm cubic voxels, or the VIPMAN phantom (Xu et al 2000), which has a voxel size of 0.3 mm x 0.3 mm x 1.0 mm. But even with these small voxels it is not possible to segment all marrow cavities, let alone RBM or BSC which occupy only a part of the volume of the cavities.
The CTN method cannot be used in this study, even if one would accept ficticious marrow voxels, because the skeletons of the MAX06 and the FAX06 phantoms have been adjusted to ICRP-based tissue distributions (Kramer et al 2006), and therefore the skeletal voxels cannot be related anymore to the grey values of the original CT images.

### 1.4 The purpose of this study

In the past, except for the investigations with the PIRT method mentioned above, skeletal dosimetry was mostly confined to the use of correction or conversion factors applied to the dosimetric results calculated in homogeneous skeletal mixtures in order to determine the equivalent dose to the RBM and the BSC, because it was not possible to model the trabecular micro structure of spongiosa in MC simulations. With the recent availability of high resolution 3D-microCT images, this limitation can be eliminated. The purpose of this study is therefore to

- propose and investigate different methods for taking into account the micro structure of spongiosa for the calculation of equivalent dose to the RBM and the BSC in the skeletons of the MAX06 and the FAX06 phantoms, and explore the minimum amount of micro-structure information required to obtain converging results.
- investigate the influence of the trabecular bone volume fraction on the results.
- compare the results with corresponding data calculated with the 3CF and the FDR methods.
- compare the results with corresponding data for other exposure models.

## 2. Materials and Methods

### 2.1 The MAX06 and the FAX06 phantoms

MAX06 and FAX06 (Kramer et al 2006) are updated versions of the MAX (Kramer et al 2003) and of the FAX phantoms (Kramer et al 2004a). The update became necessary because of the inclusion of the extrathorarcic airways, the oral mucosa, the gall bladder, the heart, the lymphatic nodes, the prostate and the salivary glands into the concept of effective dose in the future (ICRP 2006), and because the application of the 3D-microCT image-based dosimetry requires separately segmented regions of cortical bone and spongiosa. The updated phantoms are made of 1.2 mm cubic voxel, and the additional segmentation was based on the original CT images from which the MAX/FAX phantoms had been developed, on anatomical textbooks, and on skeletal data provided by ICRP70 and ICRP89

(ICRP 2002). Like MAX and FAX, the MAX06 and the FAX06 phantoms have organ and soft tissue masses in accordance with the reference data from ICRP89, but additionally these updated versions have also ICRP-based distributions of skeletal tissue volumes. Taking advantage of this opportunity, cartilage and the medular YBM in the shafts of the long bones have been segmented as well.

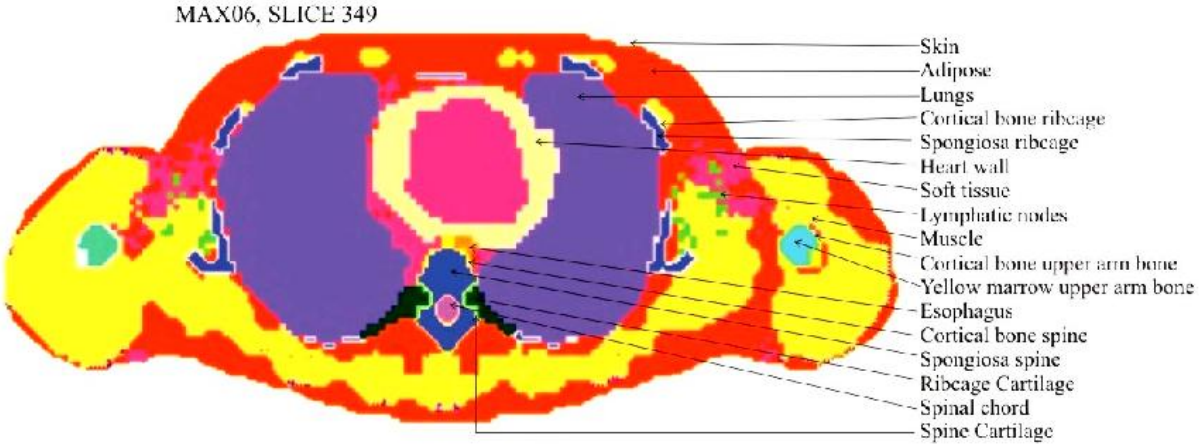


**Figure 1.** MAX06 phantom: Transversal image in the heart region

Figure 1 represents a transversal image of the MAX06 phantom showing important organs, like the lungs and the heart, and also separately segmented skeletal tissues, like cortical bone, spongiosa, cartilage and medular YBM. The complete description of the MAX06 and the FAX06 phantoms can be found elsewhere (Kramer et al 2006).

### 2.2 3D-MicroCT images of vertebral bodies

Because of the 1.2mm cubic voxels used for the MAX06 and the FAX06 phantoms, in this study a micro matrix is defined as a 1.2 mm cube of spongiosa filled with micro voxels made of segmented trabecular bone, BSC and marrow extracted from 3D-microCT scanned images. These micro matrices have been extracted from 3D-microCT images of the vertebral bodies provided by Salmon (2006), Bauer (Bauer et al 2004) and Bolch (Shah et al 2005c). Table 1 presents information as far as available about the bone specimens and the individuals from which the vertebrae have been taken post mortem.The bone specimens were obtained from donors with no medical history of metabolic bone desease or cancer and showed no radiographic evidence of damage or bone pathologies.

**Table 1.** Data of the 3D-microCT images of spongiosa

| Bone specimen | Gender | Age [y] | Height [cm] | Weight [kg] | Vertebra | Resolution [micron] | Image size $mm^3$ |
|---|---|---|---|---|---|---|---|
| S0117 | | | | | 11. thorarcic | 17.5 | 9.0 x 9.0 x 4.5 |
| B1830 | female | 68 | 170 | 70 | 8. thorarcic | 30 | 7.9 x 7.9 x 7.7 |
| B0160 | male | 66 | 173 | 68 | 4. lumbar | 60 | 12.0 x 12.9 x 8.7 |

Specimen **S0117** was provided as 800 raw images of size 2083 x 1651 each, containing spongiosa, cortical bone and cartilage, with a cubic voxel resolution of 17.5 micron. The voxel number in a 1.2 mm cubic micro matrix would be 1.2 mm / 17.5 micron = 68.57 for each dimension, which is not an integer. Therefore, the images of specimen S0117 were re-sampled to a voxel resolution of 17.64706 micron in order to yield 68 x 68 x 68 voxels per micro matrix. After the removal of noise with a

median filter, the images were segmented into trabecular bone and soft tissue. Finally a parallelepiped of spongiosa with a size of 9 mm x 9 mm x 4.5 mm was extracted from the segmented 3D-image.

Specimen **B1830** has been received as a parallelepiped of spongiosa with dimensions of 7.9 mm x 7.9 mm x 7.7 mm and already segmented into trabecular bone and soft tissue (marrow + BSC). Segmentation of the images involved first the application of a low pass Gaussian filter (width=0.5, support=1, kernel size=3x3x3) to remove noise, and then secondly the binarization into trabecular bone and soft tissue by using a single global threshold, which was selected in the middle of the two peaks of the histogram (Bauer 2004). With respect to the 1.2 mm cubic voxels in the MAX and FAX skeletons, the voxel resolution of specimen B1830 yielded 40 x 40 x 40 voxels per micro matrix.

Specimen **B0160** arrived also as a parallelepiped of spongiosa with dimensions of 12 mm x 12.9 mm x 8.7 mm extracted from the vertebral body and segmented into trabecular bone and soft tissue (marrow + BSC). The segmentation process included the following steps (Rajon et al 2006):

- median filtration with kernel size 3x3x3 to remove noise,
- thresholding using image-gradient inspection
- segmentation into binary images of trabecular bone and soft tissue.

The micro matrix dimensions based on specimen B0160 were 20 x 20 x 20.

BSC segmentation

Finally the BSC were segmented in the soft tissue of all bone specimens from table 1 as the first voxel layer covering the surfaces of trabecular bone, with the remaining soft tissue micro voxels representing marrow.
If a 3D-microCT image would have a voxel resolution of 10 micron, the BSC equivalent dose could be calculated as the average equivalent dose in the first voxel layer covering the surfaces of trabecular bone. For voxel resolutions greater than 10 micron one would have to introduce an algorithm into the MC code, which determines the distance between the location of the particle's interaction and the bone surface in the first voxel layer and then deposits the energy either in BSC or marrow, depending on the decision if this distance is smaller equal or greater than 10 micron. As three different voxel resolutions were available here, this study applies a different approach. Depending on the voxel resolution of the bone specimen used in the MC calculation, the BSC equivalent dose will be determined as the equivalent dose to soft tissue adjacent to the trabecular bone surface averaged over a thickness of 17.65, 30 and 60 micron, respectively. These data will then be used to obtain the BSC equivalent dose for the recommended thickness of 10 micron by extrapolation.

## Voxel effects

The interface between two different tissues is normally a curved surface, whereas voxels used in digital imaging have a rectangular shape. Consequently, in digital 3D images this curved surface runs through some of the voxels which then represent a mixture of both tissues. This phenomenon is referred to as the partial volume effect. The dosimetric consequence of the partial volume effect for bone-marrow interfaces segmented based on cubic voxels and then exposed to electrons emitted by radionuclides concentrated in trabecular bone or marrow has been called "voxel effect" and has been studied extensively by Rajon et al (2000, 2002a, 2002b). For a simple model based on spheres embedded in cubes, voxel effects which cause an overestimation of the cross absorbed fraction or the cross absorbed dose in marrow were found to be noticeable only when the range of the electrons in marrow is smaller than the voxel size, i.e. for cubic voxel sizes smaller than 100 micron the energy of the electrons would have to be less than 50 keV. In particular it was found that the relative error in the S values in the marrow cavities from electrons emitted in trabecular bone, calculated for five radionuclides of interest in skeletal dosimetry, were less than 5% for cubic voxel sizes smaller than 100 micron. Rajon et al's studies of the influence of voxel effects on S values represent important investigations, because marrow toxicity is a major concern in nuclear medicine, especially when bone-seeking radionuclides are used for the therapy of bone cancer.

This study is using the MAX06 and the FAX06 phantoms exposed to external photons covering the whole body to determine the equivalent doses to the RBM and the BSC, for the time being mainly for the purposes of radiation protection for occupational and environmental exposures. Electrons liberated by photons in the marrow cavities are the main contributor to the equivalent dose for all incident photon energies, while photo-electrons released in neighbouring trabecular bone additionally increase the equivalent dose in the marrow cavity significantly only for incident photon energies up to 150 keV, i.e. predominantly in region close to the bone surface. Based on the cubic voxel sizes of 17.65, 30 and 60 micron used in this study, voxel effects from electrons released in trabecular bone according to Rajon et al would be noticeable only for electron energies below 30, 40 and 60 keV, respectively, though not for the RBM but here only for the BSC equivalent dose, because the BSC thickness was segmented as the first voxel layer on the surface of trabecular bone. Actually, the question is whether one would see a significant dosimetric impact on the BSC equivalent dose from voxel effects at all, because here electrons also originate in the BSC layer, which suggests that the voxel effects related to electrons originating on the one hand in trabecular bone and on the other hand in the BSC voxel layer would at least partly cancel out. Under these circumstances one can assume that uncertainties for the whole-body BSC equivalent dose from voxel effects for the exposure conditions considered here would not exceed the 5% found for the S values in the studies of Rajon et al. While it is intended to make a more detailed investigation of voxel effects for skeletal dosimetry in the MAX06 and the FAX06 phantoms with respect to nuclear medicine applications in the future this is considered to be beyond the scope of this paper.

### 2.3 3D-microCT images for a complete human skeleton

The thickness of the trabeculae and the size of the soft tissue filled cavities can vary significantly among different bones of the human skeleton. In order to get a data set of micro matrices to be used for all bones of the MAX06 and the FAX06 skeletons, the volume fractions of trabecular bone in the 3D-microCT images of spongiosa mentioned in table 1 have been changed according to data extracted from table 15 of ICRP Report 70 (ICRP 1995), which apply to adults of age 41 to 50 and are shown here in table 2. This was achieved by an algorithm which increased or decreased uniformly the number of trabecular bone voxels on the surface of the existing trabecular bone until the desired volume fraction was established. By this method five derived 3D-microCT images with 10, 12, 15, 20 and 55% trabecular bone volume have been created for each of the three bone specimens mentioned in table 1. It would have been better, of course, to use specimens from different bone sites, but unfortunately those were not available for this study. On the other hand it will be shown below that percentage variations of the trabecular bone volume between 10 and 20% for all bones, except the skull, have only a small effect on the whole-body RBM and BSC equivalent doses.

**Table 2.** Bone-specific trabecular volume fractions in spongiosa based on ICRP70

| Adult<br>Skeletal region | trab. volume frac.<br>% |
|---|---|
| Arm bones | 15 |
| Ribcage | 10 |
| Spine | 12 |
| Skull | 55 |
| Mandible | 55 |
| Pelvis | 20 |
| Leg bones | 15 |

## 2.4 Skeletal dosimetry with clusters of micro matrices

The MAX06 and the FAX06 phantoms have about 2 million and 1.5 million 1.2 mm cubic spongiosa voxels, respectively. Applying the 3D-microCT images of spongiosa to skeletal dosimetry one might think at first about filling these millions of spongiosa macro voxels of a human skeleton with different micro matrices made of segmented marrow, BSC and trabecular bone. However, apart from the expenditure of coding millions of micro matrices, this would lead to an explosion of memory space and execution time of the MC code.

Instead, this study suggests to calculate the equivalent dose to the RBM and the BSC in the spongiosa of the MAX06 and the FAX06 phantoms based on a cluster (= a parallelepiped made of a small number) of micro matrices for each of the five trabecular bone volume fraction observing the following conditions:

a) The cluster of micro matrices must be selected from the 3D-microCT image in such a way that the trabecular bone volume fraction of the cluster is equal to that of the whole 3D-microCT image.
b) The number of micro matrices of the cluster can be reduced as long as the equivalent doses to the RBM and the BSC do not change within the margins of the statistical errors, and condition a) is still met.

For the calculations to be presented in the next chapter clusters of 4, 6, 8, 12 and 27 1.2 mm cubic micro matrices have been extracted from each of the five 3D-microCT images with trabecular bone fractions of 10, 12, 15, 20 and 55%.

Two different methods of selecting micro matrices from the cluster at run time have been coded in the MC code:

RANDOM selection

Everytime when a particle enters a spongiosa voxel the transport is transferred to a micro matrix made of trabecular bone cavities filled with marrow and BSC, randomly selected from the cluster. The main advantage of this method is its simplicity. Its main disadvantage is the fact that the distinct cavity structure of the cluster is not preserved.

SYSTEMATIC-PERIODIC selection

Supposing the spongiosa of the skeleton is filled with the micro matrices of the cluster, then everytime when a particle enters a spongiosa voxel coming from a cortical bone voxel the transport is transferred to a micro matrix made of trabecular bone cavities filled with marrow and BSC, whose matrix index (= its position in the cluster) is selected depending on the particle's position in the phantom's macro matrix and in the cluster. However, when a particle travels from one spongiosa voxel to another, then the index of the micro matrix is determined as the index of the neighbouring micro matrix in the cluster, or the algorithm assumes that the micro matrices repeat periodically if the particle leaves the cluster. The SYSTEMATIC-PERIODIC selection maintains coherently the micro structure of the cluster as extracted from the 3D-microCT image, but this method requires a far more complex algorithm compared to the one used for the RANDOM selection.

Therefore, if for a cluster with a minimum number of micro matrices conditions a) and b) above are met, and if the results obtained for the RBM and the BSC with the two selection methods agree, then one can use this cluster with RANDOM selection for a dosimetrically adequate determination of equivalent dose to the RBM and the BSC in the skeleton.

Figure 2 gives a graphic description of the application of the cluster method for skeletal dosimetry in spongiosa voxels, here with 8 micro matrices, each of which is a 1.2mm cube, extracted from a 3D-microCT image scanned at a resolution of 30 micron having 15% trabecular bone volume. The first

step of the procedure is to extract a cluster of 8 micro matrices from the 3D-microCT image in such a way that the trabecular bone volume fraction of 15% is preserved. At runtime, when a particle enters a spongiosa voxel, two different methods of selecting a micro matrix are possible:
The RANDOM selection uses randomly one of the 8 micro matrices. The SYSTEMATIC selection chooses the first micro matrix of the cluster, and if the particle continues its path in a neighbouring spongiosa voxel, then a neighbouring micro matrix in the cluster is selected taking into account the direction of the particle's path. If the particle crosses through more than two neighbouring spongiosa voxels, then the cluster is repeated.

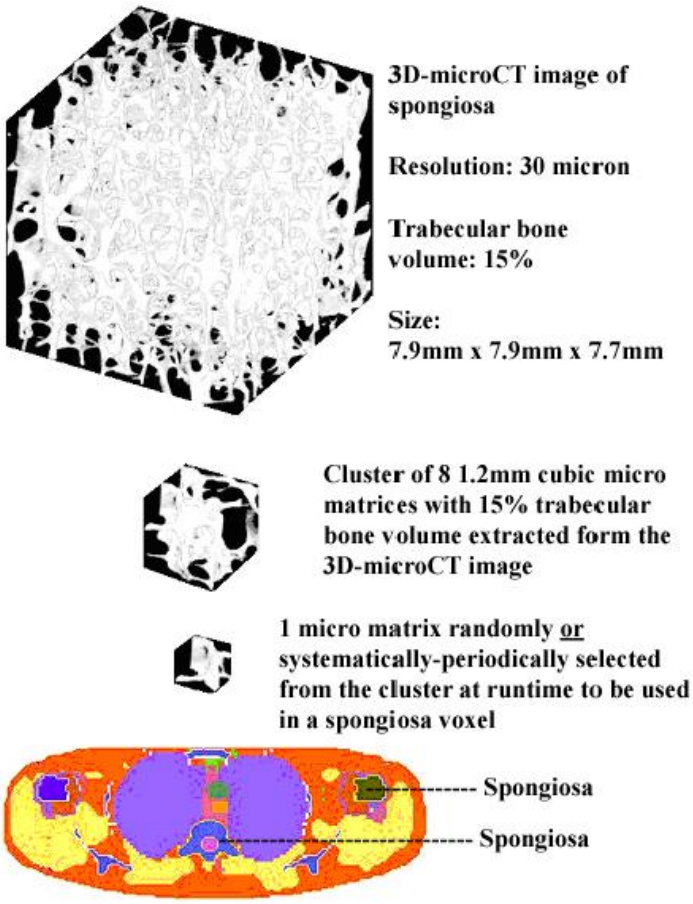


**Figure 2.** The use of a cluster of 8 micro matrices with 15% trabecular bone volume extracted from a 3D-microCT image scanned at a resolution of 30 micron for skeletal dosimetry in spongiosa.

### 2.5 Skeletal soft tissues masses

**Table 3.** Masses for RBM and YBM (ICRP 2002) and derived masses for RBM, YBM and BSC based on 10 micron BSC thickness

| Skeletal soft tissues | REF MALE m [g] | REF FEMALE m [g] | MALE m [g] | FEMALE m [g] |
|---|---|---|---|---|
| Red BM | 1170 | 900 | 1128.6 | 868.3 |
| Yellow BM | 2480 | 1800 | 1814.9 | 1333.3 |
| BSC (10 micron) | | | 108.2 | 80.4 |
| Yellow BM (medular) | | | 598.3 | 418.0 |
| Total | 3650 | 2700 | 3650 | 2700 |

The masses of RBM and YBM as defined by ICRP89 for the reference adult male and female are shown in columns 2 and 3 of table 3. Unfortunately neither ICRP89 nor ICRP70 recommend reference masses for the BSC. However, if one uses the total surface area of trabecular bone of 10.5 $m^2$ recommended by ICRP89 for the reference adult male, and the thickness of 10 micron for the BSC recommended by ICRP30 (ICRP 1979), one can calculate the total volume of the BSC for the adult male to be 105 $cm^3$, which corrsponds to a total mass of 108.2 g, assuming that the density of 1.03 g $cm^{-3}$ for the RBM (ICRU 1989) applies also to the BSC, and that all BSC are located at the surfaces of trabecular bone. At the time when this paper was written the ICRP was still looking into the posssibility to include additionally a part of cortical bone surfaces in the region of medular YBM into the volume relevant for the BSC (Eckerman 2006). In this study, however, BSC is considered only in the trabecular bone regions, i.e. only in spongiosa.

Based on the total skeletal reference masses of 10500 g for the adult male, and 7800 g for the adult female (ICRP 2002), the total mass of the BSC for the adult female would then be 108.2 g x (7800/10500) = 80.4 g. Elsewhere it was shown that the masses of medular YBM, i.e. of the YBM in the shafts of the long bones, for the adult male and female are ca. 598.3 g and 418.0 g, respectively (Kramer et al 2006). Subtracting the 598.3 g of medular YBM from the 2480g given in column 2 of table 3 yields 1881.7 g, or a total male soft tissue mass of 1170 g + 1881.7 g = 3051.7 g in the spongiosa region, with a RBM mass fraction of 1170 g/3051.7g = 0.383, and a YBM mass fraction of 1881.7 g/3051.7 g = 0.617. Now the BSC mass of 108.2 g is subtracted from the RBM and from the YBM mass of the spongiosa according to their mass fractions to give the numbers shown in column 4 of table 3. In a similar manner the numbers for the adult female in column 5 of table 3 have been calculated.

Table 4 shows the RBM and the BSC masses determined by the MC code based on the segmented 3D-microCT images. Because of the segmentation method for the BSC mentioned above, the BSC mass increases with increasing voxel size, while the RBM mass decreases correspondingly.

**Table 4.** Real RBM and BSC masses for the MAX06 and the FAX06 skeletons calculated with the cluster method for BSC thicknesses of 17.65, 30 and 60 micron.

| BONE SPECIMEN | MAX06 RBM m [g] | MAX06 BSC m [g] | FAX06 RBM m [g] | FAX06 BSC m [g] | BSC Thickness [micron] |
|---|---|---|---|---|---|
| S0117 | 1126.0 | 105.5 | 783.5 | 77.3 | 17.65 |
| B1830 | 1080.8 | 234.1 | 750.6 | 171.9 | 30 |
| B0160 | 989.8 | 436.8 | 705.3 | 320.7 | 60 |

### 2.6 EGSnrc implementation of skeletal dosimetry

So far equivalent dose calculations (Kramer et al 2003, 2004a,b, 2005) with the MAX and the FAX phantoms have been performed using the EGS4 MC code (Nelson et al 1985). The update with respect to the phantoms will be accompanied by an update with respect to the use of the MC code. Starting with this publication, equivalent or absorbed dose calculations in the MAX06 and the FAX06 phantoms use the EGSnrc MC code (Kawrakow 2000, Kawrakow and Rogers 2003), currently in the form of version V4-r2-2-3 (Kawrakow 2006). According to the requirements for the use of the EGSnrc code, three usercodes have been developed.

Usercode **3CF** applies the 3CF method as described above to calculate the equivalent dose to the RBM in a homogeneous skeleton, which means that for this method to work, cortical bone, spongiosa and

medular YBM voxels must have the same average skeletal mixture with a density of 1.4 g $cm^{-3}$ and the elemental composition taken from Cristy and Eckerman (1987). Every time when an energy deposition takes place in a skeletal voxel, a subroutine is called, which applies the three correction factors to the energy to be deposited and adds the result to the RBM bin. The masses of the RBM for both phantoms were taken from columns 4 and 5 of table 3, because according to ICRP (ICRP 1979) the thickness of BSC is considered to be 10 micron.

Usercode **FDR** applies the FDR functions taken from Cristy and Eckerman (1987) as described earlier to calculate the equivalent dose to the RBM and the BSC in a homogeneous skeleton, which means that, like for the 3CF method mentioned above, cortical bone, spongiosa and medular YBM voxels have the same average skeletal mixture with a density of 1.4 g $cm^{-3}$ and the elemental composition taken from Cristy and Eckerman (1987). The determination of the the photon fluence in the skeletal voxels is based on the track-lengths of the particles in those voxels. The masses of the RBM and the BSC were taken from columns 4 and 5 of table 3.

Usercode **MICRO** applies 3D-microCT image-based dosimetry to the skeletons. Apart from the phantom's macro matrix with ca. 150 Million 1.2 mm voxels also used in the **3CF** and the **FDR** codes, the **MICRO** code has additionally micro matrices with 314432, 64000 or 8000 voxels each, according to the cubic micro voxel dimensions of 17.65, 30 or 60 micron, respectively. For external exposures considered here, the transport of the particles begins always in the macro matrix of the phantom, i.e. the particle travels initially in an environment of 1.2 mm cubic voxels. If EGSnrc detects that a particle enters a spongiosa voxel, the transport is transferred to one of the micro matrices, according to the specific bone in which the particle is moving, and depending on the selction method chosen. Then the particle travels in an environment of 17.65, 30 or 60 micron cubic voxels, respectively. When leaving the micro matrix the particle continues its trip in a neighbouring voxel, which can be cortical bone, in this case the transport is re-transferred to the macro matrix, or which can be again a spongiosa voxel, which means the transport in another micro matrix continues.The energy deposition takes place in segmented BSC or marrow voxels. To get the energy deposited in RBM, the energy deposited in the marrow voxels is multiplied by a cellularity factor, which represents the RBM volume fraction in the marrow (ICRP 1995). The masses used for the RBM and the BSC are those shown in table 5, which have been calculated by the MC code at run time.

All calculations have been done for a large radiation field covering the entire body of the phantoms for an external parallel beam of photons with incident energies between 10 keV and 10 MeV. The direction of incidence was anterior-posterior (AP). Usercodes **3CF** and **FDR** have been run with kerma approximation and a photon cut-off energy of 2 keV, whereas usercode **MICRO** used the same photon cut-off energy, but 5 keV electron cut-off energy in cortical bone, trabecular bone, marrow and BSC, and 550 keV in all other tissues surrounding the skeleton, because electrons with kinetic energy less than 550 keV cannot cross through 1.2mm cortical bone voxels which surround the spongiosa voxels. The number of primary particles varied between 5 and 20 million per energy point in order to get a coefficient of variance (CV) for the RBM and the BSC of less than 1%.

## 3. Results and Discussions

Equivalent dose to the RBM and the BSC in the skeletons of the MAX06 and the FAX06 phantoms have been determined with the EGSnrc MC code for external exposure to photons as function of the incident photon energy for AP-incidence with a large field covering the whole body. The results in this chapter are presented in four sections: First the determination of the adequate cluster size and the selection method, second the application of random selection from 8 micro matrices for all three bone specimens, third the investigation of the influence of the trabecular bone volume fraction, fourth the comparison with the 3CF and the FDR method, and finally the comparison with data determined for other human phantoms.

### 3.1 Cluster size and selection method

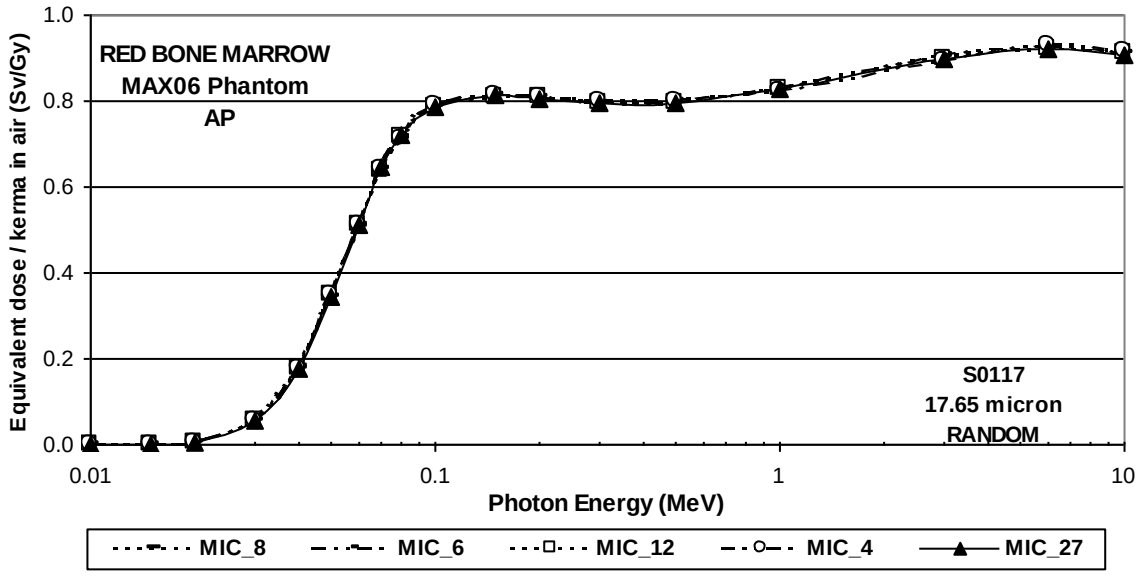


**Figure 3a.** RBM equivalent dose per air kerma free-in-air as a function of the photon energy for AP-incidence for bone specimen S0117 with 4, 6, 8, 12 and 27 micro matrices **randomly** selected

For the bone specimens S0117, B1830 and B0160 clusters with 4, 6, 8, 12 and 27 micro matrices have been extracted from each of the derived 3D-microCT images mentioned in section 2.3, maintaining 10, 12, 15, 20 and 55% trabecular bone volume in each cluster, respectively. Equivalent dose per air kerma for the RBM and for the BSC were calculated for micro matrices in spongiosa voxels randomly (RANDOM) or systematically-periodically (SYSTEMATIC) selected from the corresponding clusters for all bone specimens connected to the MAX06 and the FAX06 phantoms.

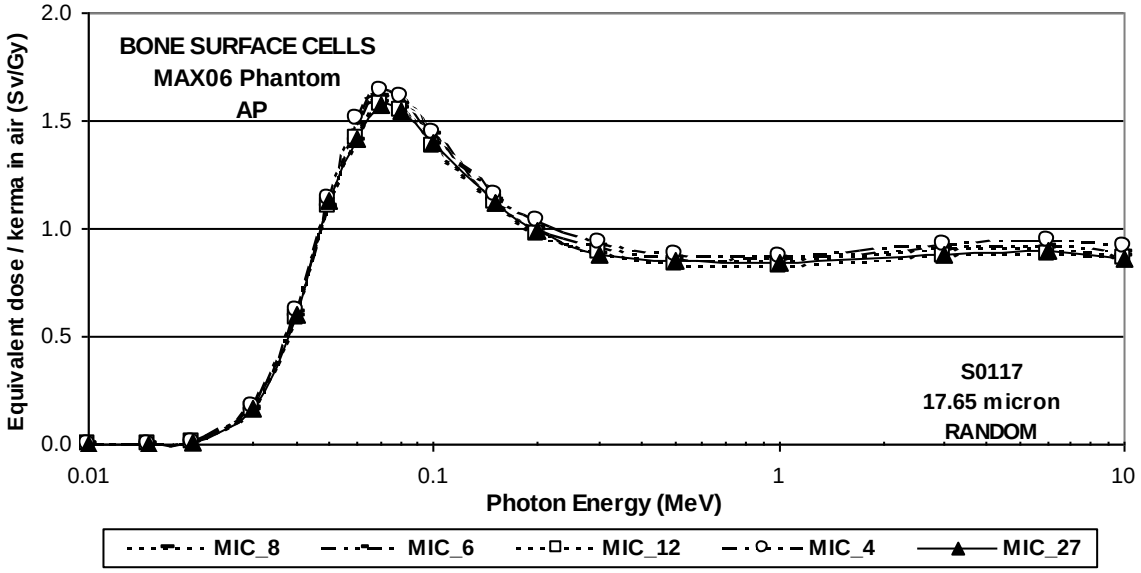


**Figure 3b.** BSC equivalent dose per air kerma free-in-air as a function of the photon energy for AP-incidence for bone specimen S0117 with 4, 6, 8, 12 and 27 micro matrices **randomly** selected

With respect to the influence of the cluster size and the selection method, results are shown only for the bone specimen S0117 connected to the MAX06 phantom, because all other combinations of bone specimens and phantoms gave consistently similar results. For the MAX06 phantom figure 3a presents the equivalent dose to the RBM per air kerma as a function of the incident photon energy for AP-incidence for selection method RANDOM for clusters of 4, 6, 8, 12 and 27 micro matrices based on bone specimen S0117 with a voxel resolution of 17.65 micron. The data for all curves agree over the whole range of energies within a margin of 2%, which is two times the maximum CV associated with each curve. For the same exposure conditions and for selection method RANDOM figure 3b shows the equivalent dose to the BSC. The curves for 8, 12 and 27 micro matrices per cluster still agree within the 2% margin, whereas the data for 4 and 6 micro matrices per cluster exceed the other curves by up to 7%. Compared to the RBM, below ca. 200 keV the BSC equivalent doses are greater and show a peak around 70 keV of incident photon energy which reflects the contribution of photo-electrons released in trabecular bone to the equivalent dose in the soft tissue voxel layer adjacent to bone.

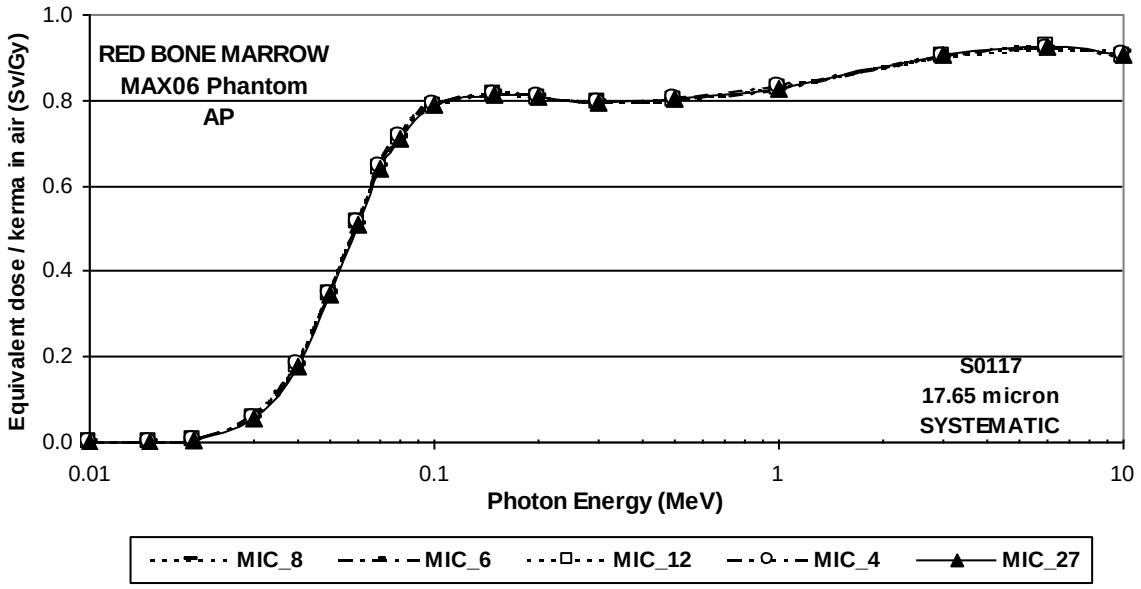


**Figure 4a.** RBM equivalent dose per air kerma free-in-air as a function of the photon energy for AP-incidence for bone specimen S0117 with 4, 6, 8, 12 and 27 micro matrices **systematically** selected

Figures 4a and 4b show corresponding data for selection method SYSTEMATIC. Again one finds agreement between the curves for all clusters for the RBM within a margin of 2%, whereas the data for 4 and 6 micro matrices per cluster for the BSC exceed the other curves here by up to 8%. Interpretation of the data shown in figures 3a to 4b suggest that a cluster of 8 micro matrices is sufficient to reach the convergence value, i.e. that the equivalent doses for RBM and BSC do not change if one increases the number of micro matrices in the cluster above eight. This is confirmed by figures 5a and 5b which demonstrate the agreement of the equivalent dose for the RBM and the BSC for the two selection methods RANDOM and SYSTEMATIC based on a cluster of 8 micro matrices.

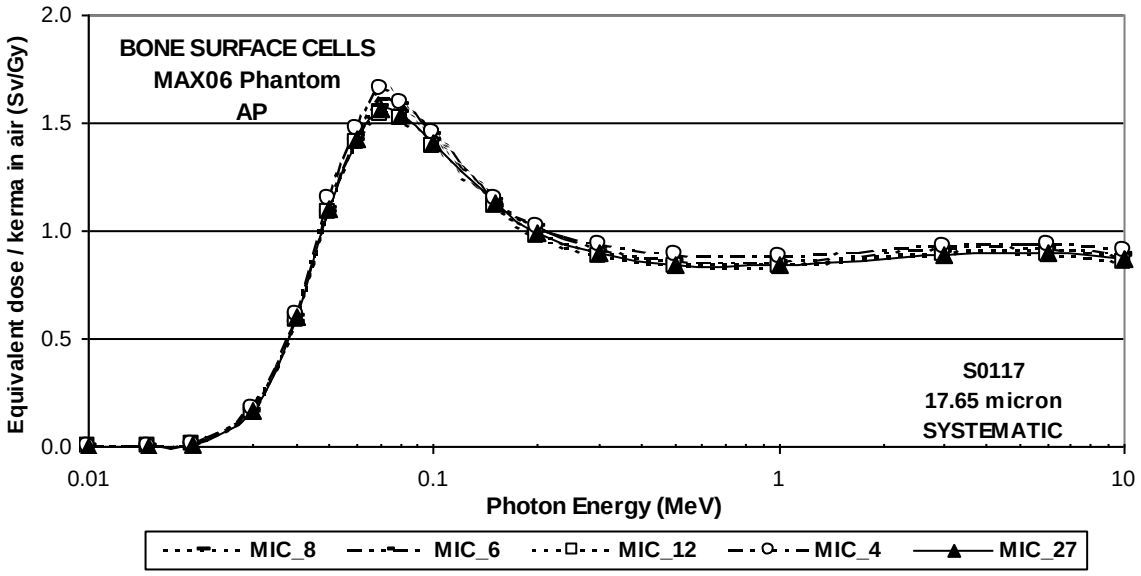


**Figure 4b.** BSC equivalent dose per air kerma free-in-air as a function of the photon energy for AP-incidence for bone specimen S0117 with 4, 6, 8, 12 and 27 micro matrices **systematically** selected

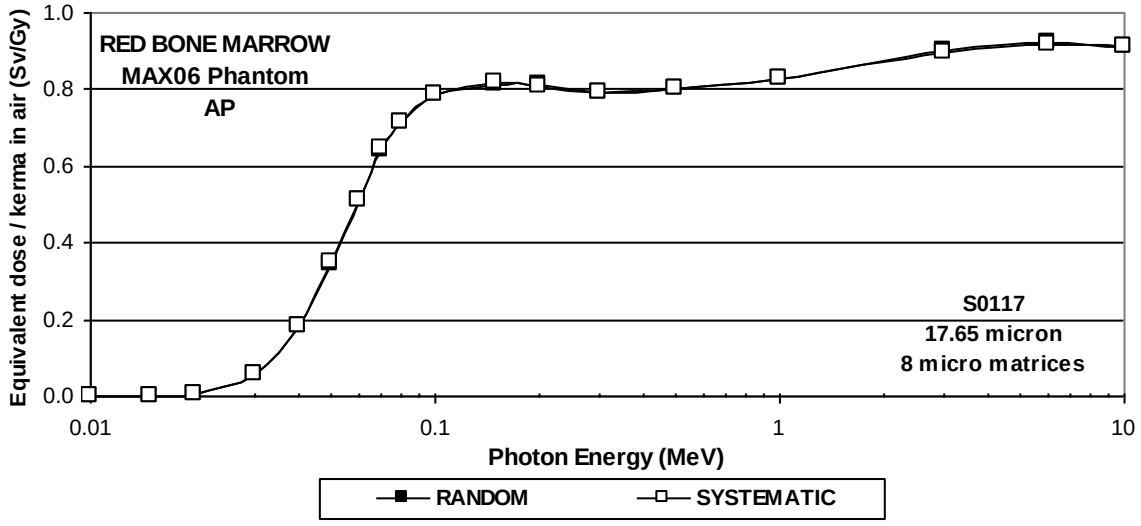


**Figure 5a.** RBM equivalent dose per air kerma free-in-air as a function of the photon energy for AP-incidence for bone specimen S0117 with 8 micro matrices **randomly** or **systematically** selected

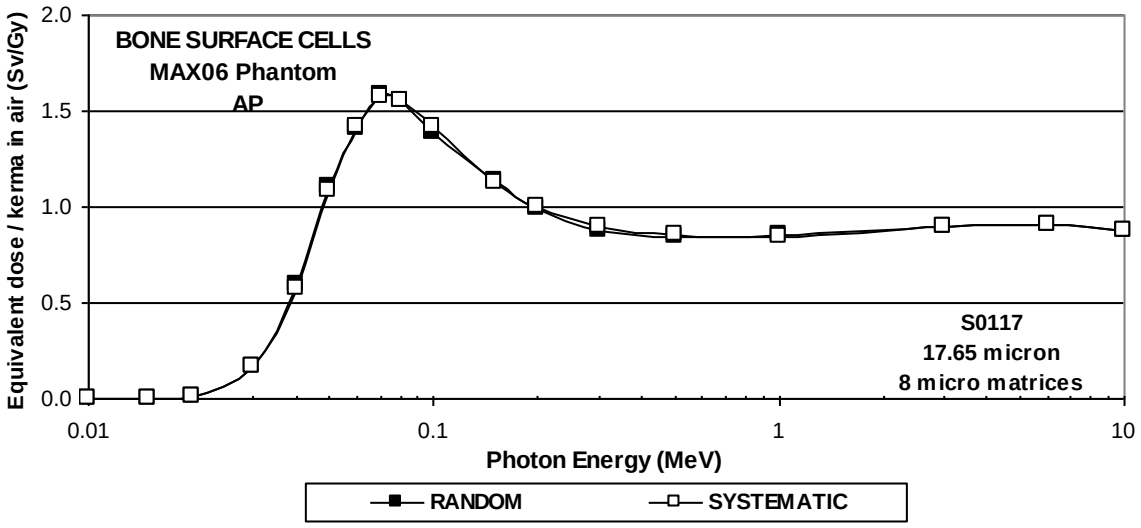


**Figure 5b.** BSC equivalent dose per air kerma free-in-air as a function of the photon energy for AP-incidence for bone specimen S0117 with 8 micro matrices **randomly** or **systematically** selected

### 3.2 Cluster with 8 micro matrices for all bone specimens

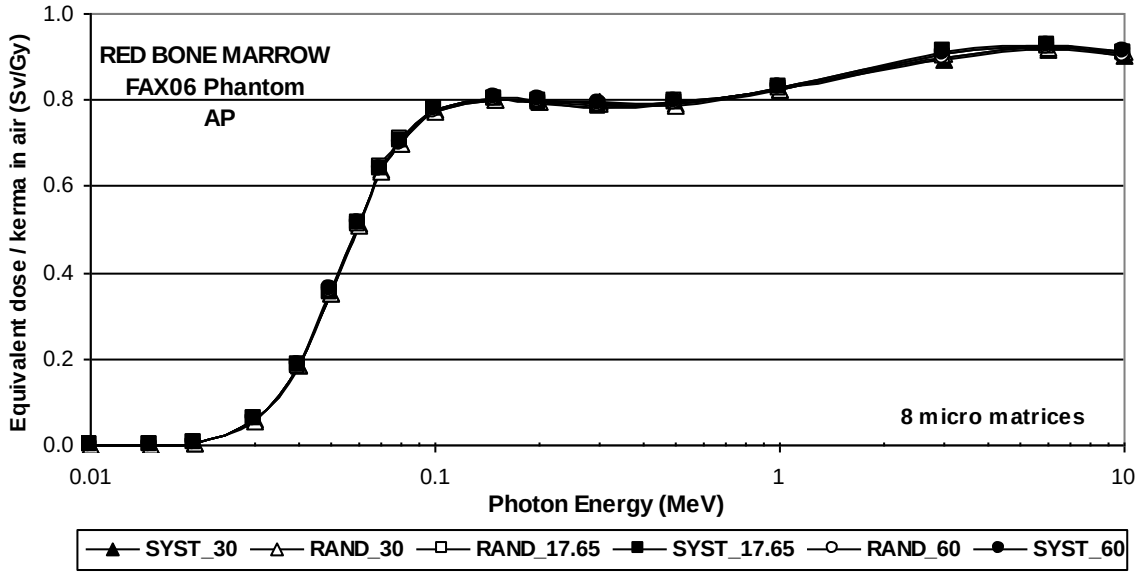


**Figure 6a.** RBM equivalent dose per air kerma free-in-air as a function of the photon energy for AP-incidence in the FAX06 phantom for all bone specimens with 8 micro matrices **randomly** and **systematically** selected for 17.65, 30 and 60 micron voxel resolution

Figure 6a shows that the voxel resolution and the selection method do not influence the equivalent dose to the RBM, at least for the resolutions and exposure condition considered here. This is due to the the average width of the marrow cavities, which has been found to be between 2200 and 650 micron for trabecular bone volume fractions between 55 and 10%. Equivalent dose to the RBM is mainly caused by electrons released by photons in the cavities, while photo-electrons with energies up to 200 keV released in trabecular bone contribute little to the equivalent dose on the other side of the first voxel layer in the cavity because of their limited range.
The equivalent dose to the BSC shown in figure 6b, however, depends strongly on the voxel resolution, because the BSC was segmented as the first voxel layer covering trabecular bone surfaces. Energy deposition in the BSC from photo-electrons released in trabecular bone for incident photon energies up to 200 keV is responsible for the equivalent dose enhancement with the typical peak around 70 keV. For a given photon energy, which is equivalent to a given range of the photo-electrons in soft tissue, this additional equivalent dose in the BSC layer decreases with increasing voxel size correspondingly to the increase of the BSC mass.

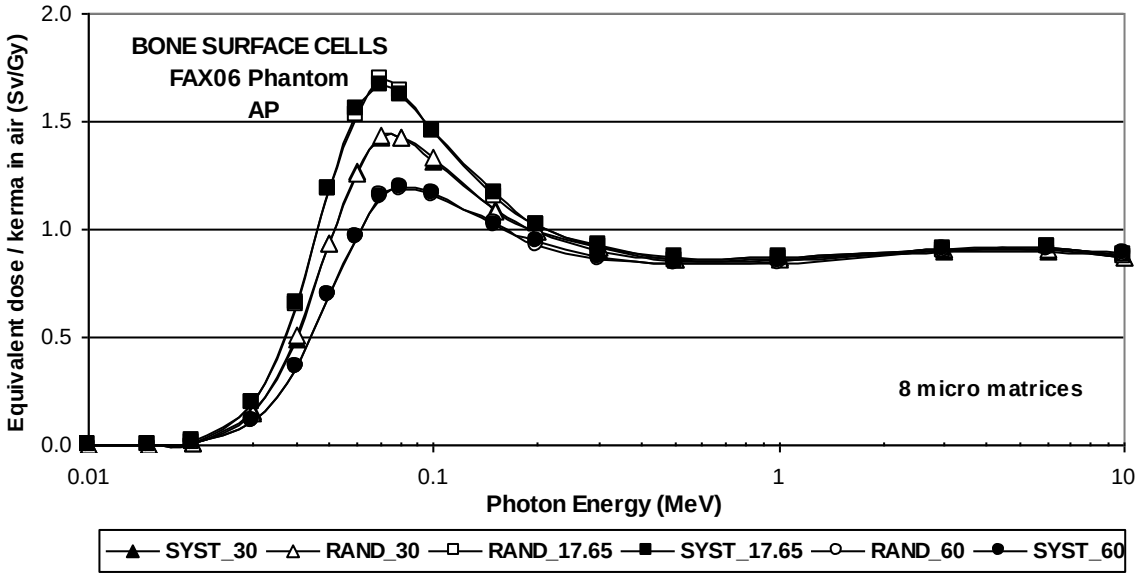


**Figure 6b.** BSC equivalent dose per air kerma free-in-air as a function of the photon energy for AP-incidence in the FAX06 phantom for all bone specimens with 8 micro matrices **randomly** and **systematically** selected for 17.65, 30 and 60 micron voxel resolution

Based on the findings of sections 3.1 and 3.2 it is justified to choose for the calculation from now on a cluster of 8 micro matrices extracted from one of the three bone specimens, and the selection method RANDOM, here called the **8R cluster method**.

### 3.3 The influence of the trabecular bone volume fraction

With respect to dosimetry a very important parameter of spongiosa is the trabecular bone volume fraction, which varies among the bones of the skeleton. Except for the skull, in all other bones the trabecular bone volume varies only between 10 and 20% according to table 2. Cristy and Eckerman (1987) suggested that equivalent doses to the RBM and the BSC obtained for a lumbar vertebra can be considered representative for the whole skeleton, except for the skull. In order to verify this assumption a calculation with 55% trabecular bone in the skull and 12% in all other bones has been

made with the 8R cluster method applied to the FAX06 phantom.Figure 7 shows RBM equivalent doses per air kerma free-in-air as a function of the photon energy for AP-incidence for the FAX06 phantom calculated with the 8R cluster method for the trabecular bone distribution mentioned in table 2, and for a distribution with 55% trabecular bone content in the skull and 12% in all other bones. Corresponding data are shown in figure 8 for the BSC.

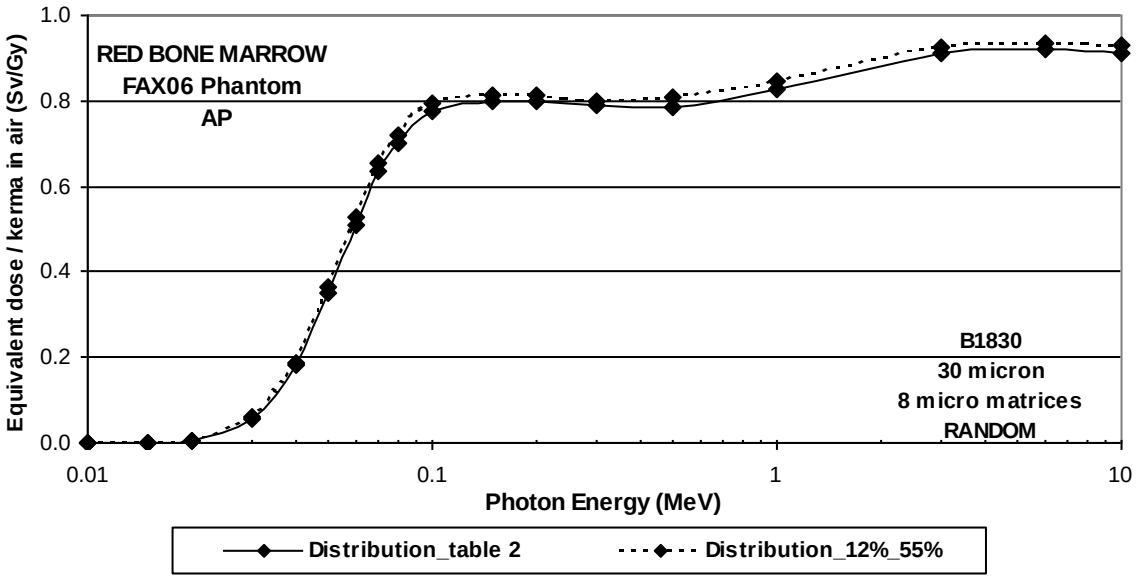


**Figure 7.** RBM equivalent dose per air kerma free-in-air as a function of the photon energy for AP-incidence for the FAX06 phantom for different distributions of trabecular bone in spongiosa

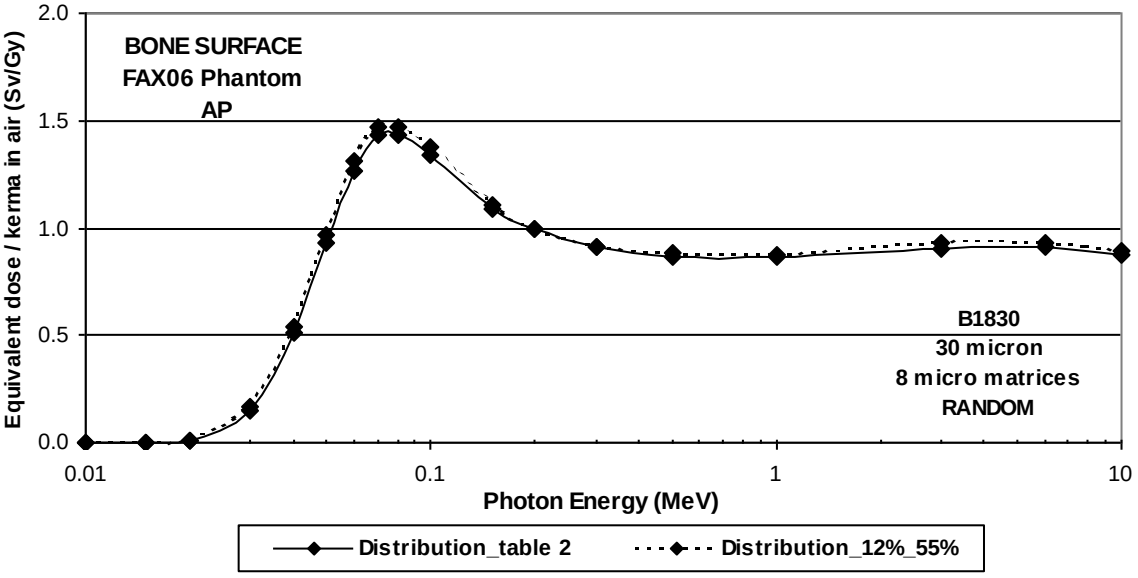


**Figure 8.** BSC equivalent dose per air kerma free-in-air as a function of the photon energy for AP-incidence for the FAX06 phantom for different distributions of trabecular bone in spongiosa

The differences between the curves for the two different trabecular bone volume distributions do not exceed 5%, thereby confirming the assumption made by Cristy and Eckerman, which suggests that all calculations could therefore be made with only two different trabecular bone volume fractions for the whole body. However, one should bare in mind that the results shown here represent whole body exposures, whereas for partial body exposures, like in X-ray diagnosis and in nuclear medicine, one would prefer to use differentiated trabecular bone volume distribution, like the one shown in table 2, for example, or even more specific distributions.

### 3.4 Comparison of the 8R cluster method with the 3CF and the FDR methods

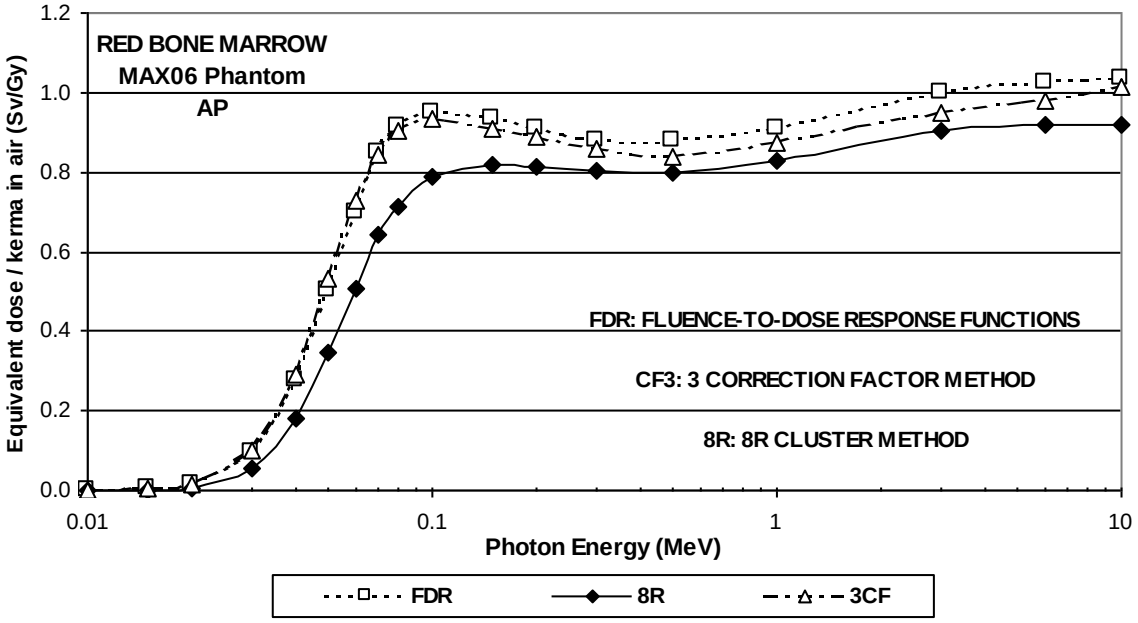


**Figure 9a.** RBM equivalent dose per air kerma free-in-air as a function of the photon energy for AP-incidence in the MAX06 phantom for different methods of skeletal dosimetry

The results of the 8R cluster method are compared in figures 9a and 10a with the results of the 3CF and the FDR method for the equivalent dose to the RBM of the MAX06 and the FAX06 phantoms. For the whole range of incident photon energies between 10 keV and 10 MeV the 3CF/FDR data are greater than the 8R cluster results. The reasons are the additional use of cortical bone and medular YBM apart from spongiosa for RBM equivalent dose calculation and the application of kerma approximation when using the 3CF/FDR methods. In contrast, the 8R cluster method calculates the equivalent dose to the RBM only in soft tissue filled cavities of spongiosa surrounded by cortical bone based on secondary electron transport. For external exposure to a real human skeleton, the radiosensitive soft tissues are shielded by cortical and to a lesser extent by trabecular bone, especially for photon energies below 500 keV. What serves as a shielding in case of a real human skeleton, becomes a region contributing to the RBM equivalent dose in the case of the homogeneous skeleton used by the 3CF/FDR methods. Figures 9a and 10a show that energy depositions by photons in "homogenized cortical bone", but also in "homogenized medular YBM" increase the equivalent dose to the RBM above the values given by the 8R cluster method. The latter considers as contributing regions only the trabecular cavities filled with marrow having densities between 0.99 and 1.02 g $cm^{-3}$ depending on the cellularity, whereas the 3CF/FDR methods use all skeletal regions with a density of

1.4 g $cm^{-3}$ as contributors to the RBM equivalent dose, which increases the equivalent dose even more. For incident photon energies above 500 keV the shielding effect of cortical bone becomes less important, because secondary electrons have increasingly enough kinetic energy to penetrate the cortical bone shielding surrounding the spongiosa voxels, and consequently the differences between the 8R cluster and the 3CF/FDR curves in figures 9a and 10a become smaller.

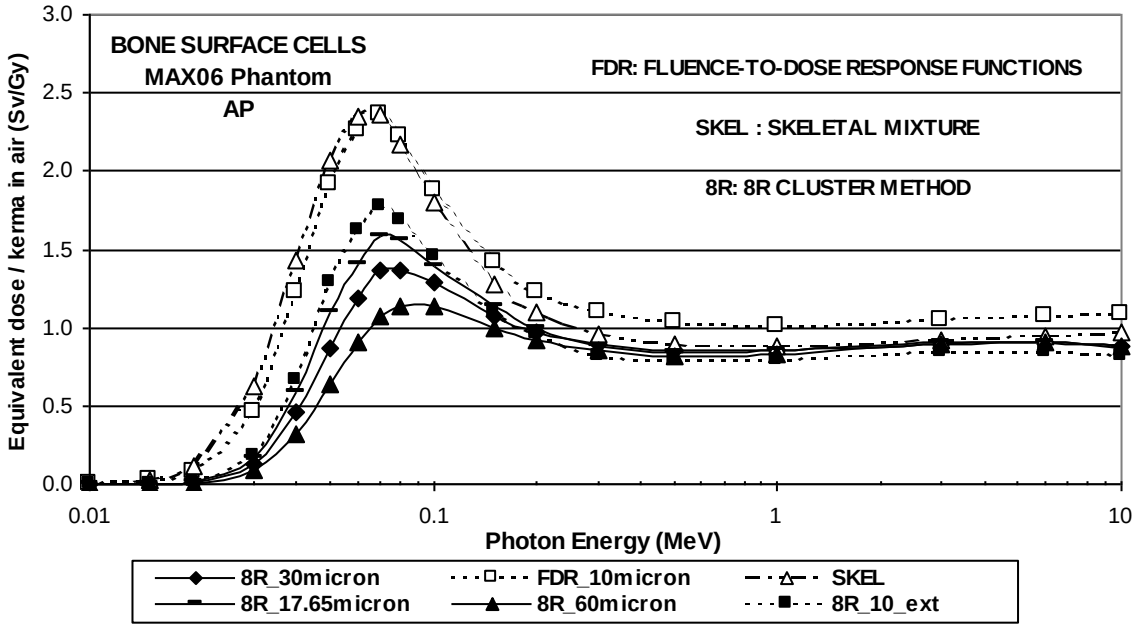


**Figure 9b.** BSC equivalent dose per air kerma free-in-air as a function of the photon energy for AP-incidence in the MAX06 phantom for different methods of skeletal dosimetry

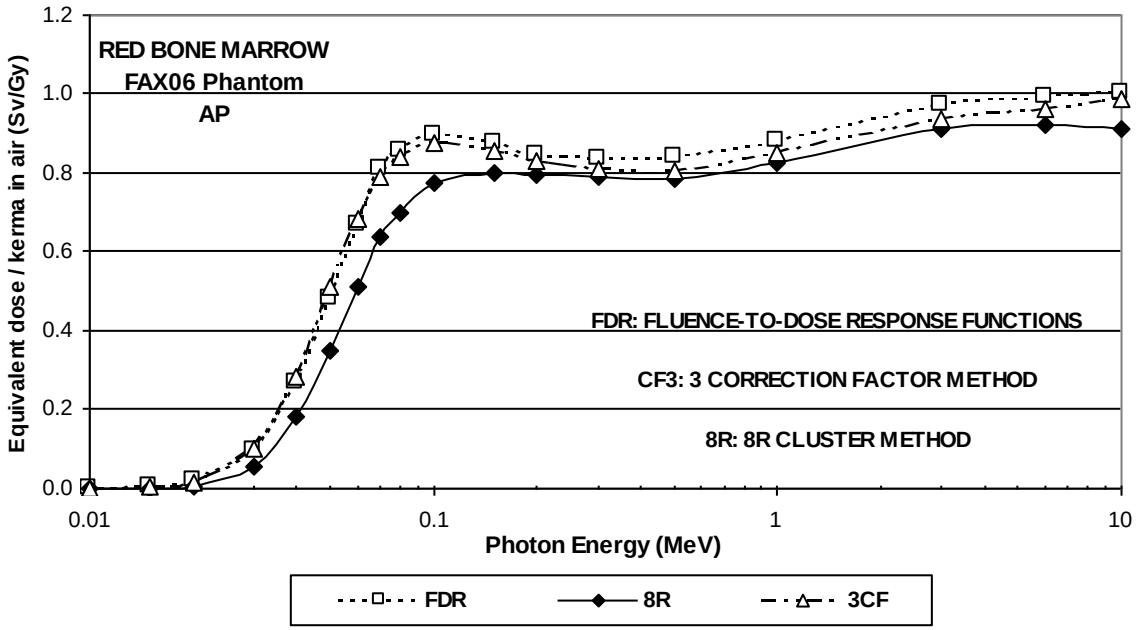


**Figure 10a.** RBM equivalent dose per air kerma free-in-air as a function of the photon energy for AP-incidence in the FAX06 phantom for different methods of skeletal dosimetry

But the 3CF/FDR data remain greater than the 8R cluster results especially when incident photon energies approach the range of 3 to 10 MeV, because the use of the kerma approximation "keeps the energy deposited in the skeleton", whereas the 8R cluster results suggest that the RBM equivalent dose from secondary electrons entering, being created in and leaving the marrow cavities remains constant or finally decreases, implicating a net electron escape from the marrow cavities with increasing energy. Differences between RBM equivalent doses calculated with the 8R cluster method and the older methods may also arise from different trabecular bone volume distributions, a fact which on the other hand may explain additionally the relatively good agreement between the 3CF and the FDR methods, because, apart from both methods using homogeneous skeletons and kerma approximation, these two methods are based on the same chord length distribution published by Darley (1968), Whitwell (1973) and Beddoe et al (1976). Explanations given above for the differences between the 8R cluster and the 3CF/FDR results apply also to the interpretation of the differences to be observed in figures 9b and 10b, which compare the BSC equivalent doses calculated with the different methods. The FDR functions for the BSC have been determined for a thickness of 10 micron, while the smallest BSC thickness used for the 8R cluster method was 17.65 micron, which additionally contributes to the increase of the FDR data.

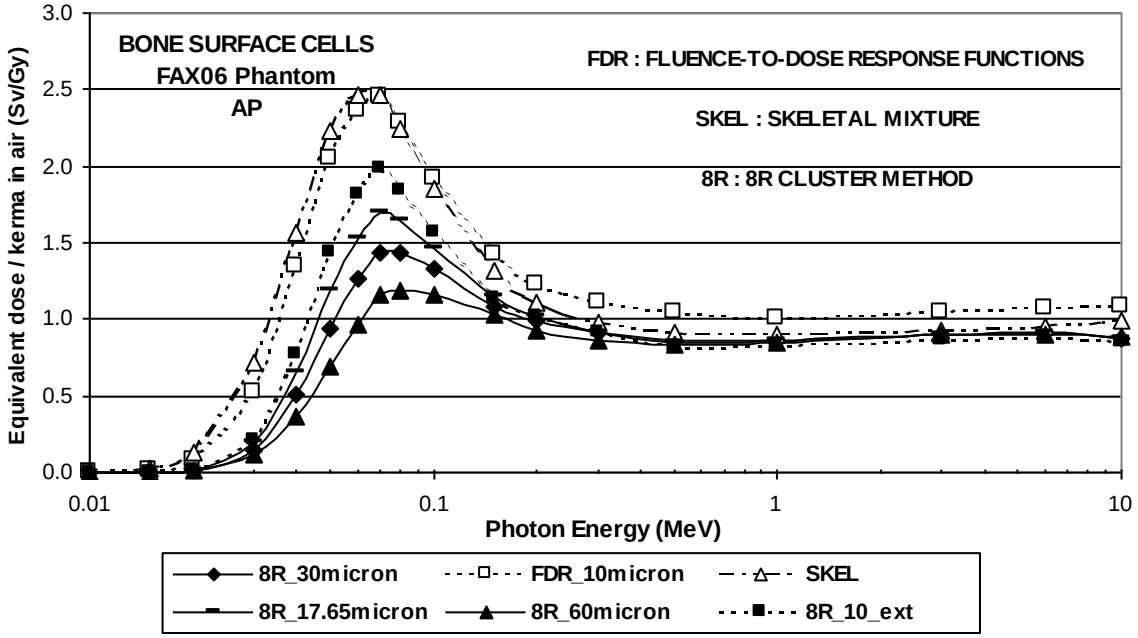


**Figure 10b.** BSC equivalent dose per air kerma free-in-air as a function of the photon energy for AP-incidence in the FAX06 phantom for different methods of skeletal dosimetry

Based on the 8R cluster results for 17.65, 30 and 60 micron the BSC equivalent dose has been extrapolated to a thickness of 10 micron, which is shown in figures 9b and 10b by the curves "8R_10_ext". But this extrapolated 10micron-curve is still well below the FDR curve. Apart from the arguments mentioned already in the discussion of the RBM results, this difference could additionally be influenced by the fact that the FDR functions for the BSC from Cristy and Eckerman (1987) take into account also cells at the surface of cortical bone, where these cells experience possibly less shielding compared to those at the surface of trabecular bone.
The "SKEL" curve represents the average equivalent dose to the homogeneous skeletal mixture which often in the past was taken as a conservative estimate for the equivalent dose to the BSC. According to the results shown in figures 9b and 10b, compared with the FDR data this assumption does not hold for energies above ca. 80 keV. Figures 9a to 10b indicate that methods based on energy deposition in all skeletal regions filled with the same average elemental composition using kerma approximation

will always overestimate the equivalent dose to the RBM and the BSC, mainly because these methods neglect the shielding effect of cortical bone for lower photon energies, and additionally the escape of secondary electrons from the trabecular cavities for higher photon energies. At least these earlier methods give a conservative estimate of the equivalent dose to the RBM and the BSC, but actually there is no need to revive these methods in the future because they use an unrealistic model of the human skeleton, and fortunately in the meantime the application of segemented 3D-microCT images in spongiosa voxel represents a more acurate alternative.

### 3.5 Comparison with RBM data for other exposure models

Figure 11 shows male RBM equivalent doses per air kerma free-in-air as a function of the photon energy for AP-incidence for the MAX06 phantom calculated with the 8R cluster method, and for the following male phantoms: MAX (Kramer et al 2003), ADAM (Zankl et al 1997), GOLEM (Zankl et al 2002), VIPMAN (Chao et al 2001) and NORMAN-05 (Ferrari and Gualdrini 2005). ADAM is a MIRD5-type mathematical phantom, while all other models are true to nature voxel-based phantoms. MAX06, MAX and NORMAN-05 have organ and tissue masses adjusted to ICRP-recommended data, whereas VIPMAN represents an adult male much taller and heavier than the ICRP reference adult male, and GOLEM has about 4 kg less whole body weight compared to the reference weight. The methods applied to the calculation of RBM equivalent dose vary significantly:

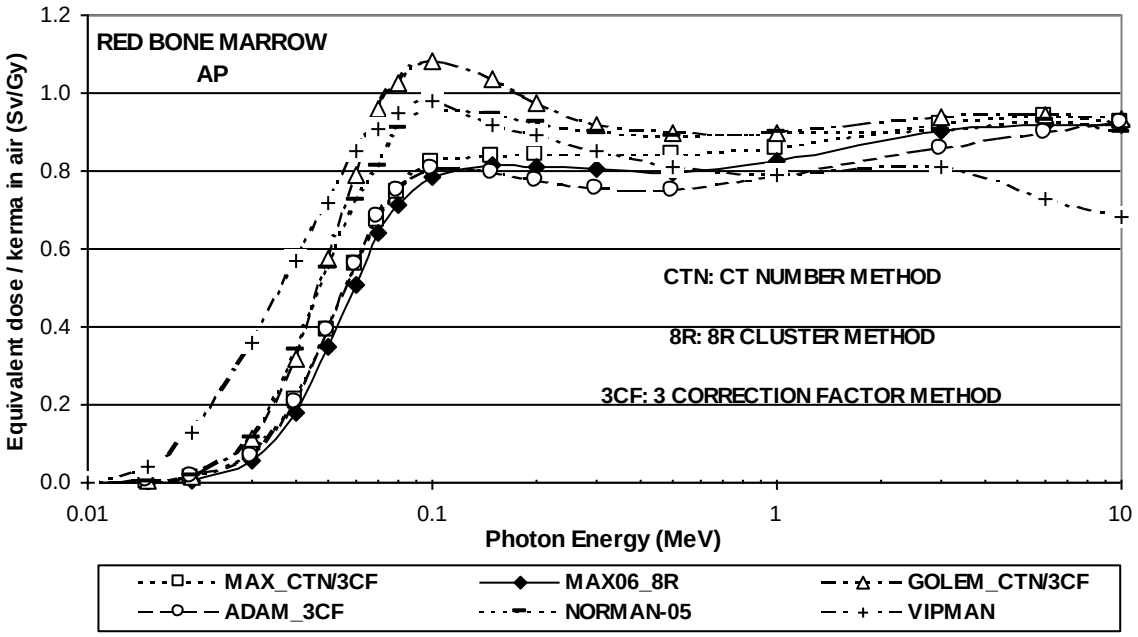


**Figure 11.** Male RBM equivalent dose per air kerma free-in-air as a function of the photon energy for AP-incidence for different male phantoms and methods of skeletal dosimetry

For the ADAM phantom the 3CF method based on early Spiers factors (Spiers 1969), and on an outdated distribution of RBM mass (ICRP 1975) was used in a homogeneous skeleton. The CTN method combined with the 3CF method using the KS factors (King and Spiers 1985) was applied to a heterogeneous skeleton in the MAX phantom, while the same method but with the older Spiers factors was used for the GOLEM phantom. For the NORMAN-5 phantom the authors developed a dose factor based on the photon energy and the MEA coefficients of RBM and the skeletal mixture to be multiplied with the photon fluence in a homogeneous skeleton with bone-specific materials taken from ICRU 46 (ICRU 1992), which actually represents some kind of FDR method.
As for the VIPMAN phantom the authors claim to have calculated the RBM equivalent dose in segmented red bone marrow voxels, which has to be questioned according to the comments made in

section 1.3.3 of this study. In addition one finds differences between tissue compositions used, as well as with regard to the use of the kerma approximation and the MC codes applied.
As for the MAX, GOLEM, ADAM and VIPMAN phantoms a comparison of their RBM equivalent doses has been discussed earlier (Kramer et al 2003), identifying for example the use of the older Spiers factors, a significantly higher calcium content in bone and less body mass as main reasons for the GOLEM RBM curve showing greater values than the MAX RBM curve. Although the CTN method has a conceptual defect as discussed in section1.3.3, the MAX curve and the MAX06 curve agree reasonably well, because both methods use heterogeneous skeletons, where spongiosa voxels are surrounded by cortical bone voxels. It seems that the shielding effect of cortical bone especially at low photon energies is mainly responsible for the MAX and the MAX06 RBM curves being well below the NORMAN-05 RBM curve, which uses a homogeneous skeleton with relatively great average skeletal densities. Reduced RBM and BSC equivalent doses due to shielding by cortical bone compared to the results from methods which use homogeneous skeletal mixtures have also been observed by Lee et al (2006) in a study on external photon exposure to different bone specimens using the PIRT method mentioned in section 1.2. In addition these authors also found good agreement between their microCT image-based method and the CTN method.

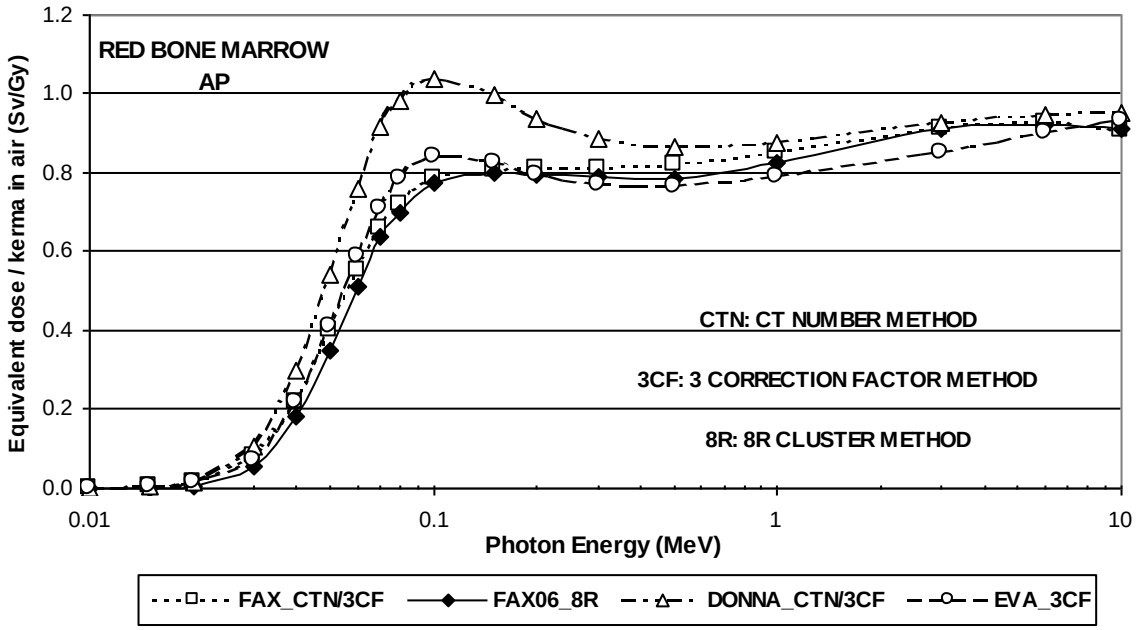


**Figure 12.** Female RBM equivalent dose per air kerma free-in-air as a function of the photon energy for AP-incidence for different male phantoms and methods of skeletal dosimetry

Figure 12 shows female RBM equivalent doses per air kerma free-in-air as a function of the photon energy for AP-incidence for the FAX06 phantom calculated with the 8R cluster method, for the FAX phantom calculated with the CTN/3CF method, and for the following female phantoms: EVA (Zankl et al 1997) and DONNA (Zankl et al 2002). The arguments of the discussion of the data for MAX06, MAX, GOLEM and ADAM in figure 11 apply basically also here for the data for FAX06, FAX, DONNA and EVA, except for the whole body mass of the DONNA phantom which is not less but significantly greater than the reference mass. Consequently the RBM equivalent dose of DONNA is less than the RBM equivalent dose of GOLEM.

## 4. Conclusions

This study proposes the cluster method for skeletal dosimetry in human phantoms to be applied to spongiosa voxels segmented in the skeleton. A cluster represents a parallelepiped extracted from a 3D-microCT image of spongiosa and divided into a certain number of micro matrices, each of which has the size of a spongiosa voxel and is segmented into trabecular bone, marrow and BSC. During MC calculations of equivalent dose distributions in human phantoms, whenever a particle enters a spongiosa voxel, the transport is transferred to one of the micro matrices, and energy deposition is registered directly in segmented BSC and marrow voxels. By applying the RANDOM as well as the SYSTEMATIC method of selecting a micro matrix at run time from clusters composed of 4 to 27 micro matrices, this study has shown that RBM and BSC equivalent doses in the skeletons of the MAX06 and the FAX06 phantoms can be calculated using a cluster of only 8 micro matrices and the RANDOM selection method, for the time being for the three bone specimens used and the exposure conditions considered here. The calculations presented here have shown in particular that the results neither depend on gender, nor on the anatomical characteristics of the donor of the bone specimen, nor on the type of vertebra selected, and also not on the segmentation technique applied. For the equivalent doses to the RBM even the voxel resolution of the 3D-microCT images was not relevant, at least for the range between 17.65 and 60 micron.

On the one hand the 3D-microCT image in figure 2 shows that the irregular form and the complex spacial distribution of the bone trabeculae and of the soft tissue filled cavities are creating an extremely inhomogeneous environment for a particle crossing through a spongiosa voxel, but on the other hand according to the results it seems, when many particles with different energies are crossing through many spongiosa voxels in many different directions, that the trabecular micro structure of the spongiosa voxels appears very similar in all directions "from the particles' point of view", which allows for the random selection from a small cluster of micro matrices in order to get dosimetrically reasonable results for equivalent dose quantities in the skeleton.
3D-microCT image-based skeletal dosimetry with the cluster method has only started. Soon the method will be applied to other exposure conditions and types of radiation relevant in radiological protection. After additional segmentation of specific bone sites within the skeletons of the MAX06 and the FAX06 phantoms, special MC codes will be developed for applications in radiology and nuclear medicine and detailed investigations of voxel effects will be carried out.

## 5. Acknowledgement

The authors want to express their gratitude to Dr. J. Bauer from the Institut fuer Roentgendiagnostik of the Technische Universitaet Muenchen, Germany, to Dr. P. Salmon from Skyscan Corporation, Belgium, to Dr. D. Rajon from the Department of Neurological Surgery and to Prof. W. Bolch, Director at the Advanced Laboratory for Radiation Dosimetry Studies (ALRADS), both from the University of Florida, USA for the 3D-microCT images of the vertebral bodies they made available for this study, and especially to Dr. D. Rajon for the patience he showed explaining the voxel effects.
Last but not least the authors want to thank Dr. A. Kramer for proposing the random selection, and for inspiring ideas which helped to find some of the bone specimens for this study.
The authors would also like to thank the Conselho Nacional de Desenvolvimento Científico e Tecnológico - CNPq and the Fundação de Amparo à Ciência do Estado de Pernambuco - FACEPE for the financial support.

## 6. References

Bauer JS, Issever AS, Fischbeck M, Burghardt A, Eckstein F, Rummeny EJ, Majumdar S, Link TM 2004 Multislice-CT for structure analysis of trabecular bone - a comparison with micro-CT and biomechanical strength *Rofo Fortschr Geb Rontgenstr Neuen Bildgeb Verfahr* **176** (5) 709-718

Beddoe A H, Darley P J and Spiers F W 1976 Measurements of Trabecular Bone Structure in Man *Phys.Med.Biol.* **21**, No 4, 569-607

Beddoe A H and Spiers F W 1979 A Comparaive Study of Bone-Seeeking Radionuclides in Man, Rhesus Monkey, Beagle, and Miniature Pig *Rad.Res.* **80**, 423-439

Bolch W E, Patton P W, Rajon D A, Shah A P, Jokisch D W and Inglis B A 2002 Considerations of Marrow Cellularity in the 3-Dimensional Dosimatric Models of the Trabecular Skeleton *J Nucl Med* **43**, No.1, 97- 108

Bouchet L G, Jokisch D W and Bolch W E 1999 A Three-Dimensional Transport Model for Dtermining Absorbed Fractions of Energy for Electrons within Trabecular Bone *J Nucl Med* **40**: 1947-1966

Chao T C, Bozkurt A, Xu X G 2001 Conversion Coefficients Based on the VIP-Man Anatomical Model and EGS4-VLSI Code for External Monoenergetic Photons from 10 keV to 10 MeV, *Health Physics* **81**(2):163-183

Cristy M and Eckerman K F 1987 Dose-Response Functions for soft tissues of the skeleton In: Specific Absorbed Fractions of Energy at Various Ages from Internal Photon Sources. I. Methods *ORNL/TM-8381/V1* Oak Ridge National Laboratory, TN, USA

Darley P J 1968 Measurements of linear path length in bone and bone marrow using a scanning technique. In: Procedings on the Symposium on Microdosimetry, EAEC Publication EUR 3747 d-e-f, pp. 509-526

Eckerman K F and Stabin M G 2000 Electron Absorbed Fractions and Dose Conversions Factors for Marrow and Bone by Skeletal Regions *Health Phys.* **78**(2): 199-214

Eckerman K F 2006 private communication, *email from March 6, 2006*

Ferrari P and Gualdrini G 2005 An improved MCNP version of the NORMAN voxel phantom for dosimetry studies, *Phys.Med.Biol*. **50** 4299-4316

ICRP 1975 Report of the Task Group on Reference Man. *ICRP Publication 23,* International Commission on Radiological Protection, Pergamon Press, Oxford

ICRP 1979 Limits for Intakes of Radionuclides by Workers *ICRP Publication 30* (Oxford: Pergamon)

ICRP 1991 1990 Recommendations of the International Commission on Radiological Protection *ICRP Publication 60* (Oxford: Pergamon)

ICRP 1995 Basic Anatomical and Physiological Data for use in Radiological Protection: The Skeleton. *ICRP Publication 70* (Oxford: Pergamon)

ICRP 2002 Basic Anatomical and Physiological Data for Use in Radiological Protection: Reference Values *ICRP Publication 89* Ann. ICRP 32 (3-4) Elsevier Science Ltd., Oxford.

ICRP 2006 Recommendations of the International Comission on Radiological Protection *Draft document 02/276/06* 5 June 2006 on: www.icrp.org

ICRU 1989 Tissue Substitutes in Radiation Dosimetry and Measurement *ICRU Report No. 44* International Commission On Radiation Units And Measurements, Bethesda, MD, USA

ICRU 1992 Photon, Electron, Proton and Neutron Interaction Data for Body Tissues *ICRU Report No. 46* International Commission On Radiation Units And Measurements, Bethesda, MD, USA

Jokisch D W, Bouchet L G, Patton P W, Rajon D A and Bolch W E 2001 Beta-particle dosimetry of the trabecular skeleton using Monte Carlo transport within 3D digital images *Med.Phys.* **28** (7), 1505-1518

Kawrakow I 2000 Accurate condensed history Monte Carlo simulation of electron transport. I. EGSnrc, the new EGS4 version, *Med.Phys.* **27**, 485-498

Kawrakow I and Rogers D.W.O. 2003 The EGSnrc code system: Monte Carlo simulation of electron and photon transport, *NRC Report PIRS-701*

Kawrakow I 2006 Version V4-r2-2-3 of the EGSnrc code system *http://www.irs.inms.nrc.ca/EGSnrc/EGSnrc.html*

King S D and Spiers F W 1985 Photoelectron enhancement of the absorbed dose from X rays to human bone marrow: experimental and theoretical studies *Br.J.Radiol.* **58**, No. 688, 345-356

Kramer R 1979 Ermittlung von Konversionsfaktoren zwischen Körperdosen und relevanten Strahlungskenngrößen bei externer Röntgen- und Gamma-Bestrahlung *GSF-Report-S-556* Institut für Strahlenschutz, GSF-Forschungszentrum für Umwelt und Gesundheit, Neuherberg-Muenchen

Kramer R, Zankl M, Williams G and Drexler G 1982 The calculation of dose from external photon exposures using reference human phantoms and Monte Carlo methods. Part I: The male

(ADAM) and female (EVA) adult mathematical phantoms *GSF-Report S-885*, Institut für Strahlenschutz, GSF-Forschungszentrum für Umwelt und Gesundheit, Neuherberg-Muenchen

Kramer R, Vieira J W, Khoury H J, Lima F R A and Fuelle D 2003 All About MAX: a Male Adult voXel Phantom for Monte Carlo Calculations in Radiation Protection Dosimetry, *Phys. Med. Biol*., **48**, No. 10, 1239-1262

Kramer R, Vieira J W, Khoury H J, Lima F R A, Loureiro E C M, Lima V J M and Hoff G 2004a All about FAX: a Female Adult voXel Phantom for Monte Carlo Calculation in Radiation Protection Dosimetry, *Phys. Med. Biol.* **49**, 5203-5216

Kramer R, Vieira J W, Khoury H J and Lima F R A 2004b MAX meets ADAM: a Dosimetric Comparison Between a Voxel-Based and a Mathematical Model for External Exposures to Photons, *Phys. Med. Biol*. **49**, 887-910

Kramer R, Khoury H J and Vieira J W 2005 Comparison between effective doses for voxel-based and stylized exposure models from photon and electron irradiation *Phys. Med. Biol* **50,** 5105-5126

Kramer R, Khoury H J, Vieira J W and Lima V J M 2006 MAX06 and FAX06: Update of two adult human phantoms for radiation protection dosimetry *Phys. Med. Biol.* **51** 3331-3346

Lee C, Lee C, Shah A P and Bolch W E 2006 An Assessment of Red Bone Marrow and Bone Endosteum Dosimetry Methods for External Photons *Phys.Med.Biol.* **51**, 5391-5408

Nelson W R, Hirayama H and Rogers D W O 1985 The EGS4 Code System *SLAC-265*, Stanford Linear Accelerator Center, Stanford University, Stanford, CA,USA

Patton P W, Rajon D A, Shah A P, Jokisch D W, Inglis B A and Bolch W E 2002 Site-specific variability in trabecular bone dosimetry: Considerations of energy loss to cortical bone *Med.Phys.* **29** (1), 6-14

Patton P W, Jokisch D W, Rajon D A, Shah A P, Myers S L, Inglis B A and Bocl W E 2002 Skeletal Dosimetry Via NMR Microscopy: Investigations of Sample Reproducibility and Signal Source *Health Phys.* **82** (3): 316-326

Rajon D A, Jokisch D W, Patton P W, Shah A P and Bolch W E 2000 Voxel size effects in three-dimensinal nuclear magnetic resonance microscopy performed for trabecular bone dosimetry *Med. Phys.* **27** (11), 2624-2635

Rajon D A, Jokisch D W, Patton P W, Shah A P, Watchman C J and Bolch W E 2002a Voxel effects within digital images of trabecular bone and their consequences on chord-length distribution measurements *Phys.Med.Biol.* **47** 1741-1759

Rajon D A, Patton P W, Shah A P, Watchman C J and Bolch W E 2002b Surface area overestimation within three-dimensional digital images and its consequences for skeletal dosimetry *Med.Phys.* **29** (5), 682-693

Rajon D A, Pichardo J C, Brindle J M, Kielar K N, Jokisch D W, Patton P W and Bolch W E 2006 Image segmentation of trabecular spongiosa by visual inspection of the gradient magnitude *Phys.Med.Biol* **51** 4447-4467

Rosenstein M 1976 Organ Doses in Diagnostic Radiology *DHEW Publication (FDA)* 76-8030

Salmon P 2006 personal communication *Skyscan Corporation*, 2630 Aartselaar, Belgium

Shah A P, Patton P W, Rajon D A and Bolch W E 2003 Adipocyte Spatial Distributions in Bone Marrow: Implications for Skeletal Dosimetry Models *J Nucl Med* **44**, No. 5, 774-783

Shah A P, Rajon D A, Jokisch D W, Patton P W and Bolch W E 2005a A Comparison of Skeletal Chord-Length Distributions in the Adult Male *Health Phys.* **89** (3): 199-215

Shah A P, Jokisch D W, Rajon D A, Watchman C J, Patton P W and Bolch W E 2005b Chord-based versus voxel-based methods of electron transport in the skeletal tissues *Med.Phys.* **32** (10), 3151-3159

Shah A P, Bolch W E, Rajon D A, Patton P W and Jokisch D W 2005c A Paired-Image Radiation Transport Model for Skeletal Dosimetry *J Nucl Med* **46**, No.2, 344-353

Shah A P, Rajon D A, Patton P W, Jokisch D W and Bolch W E 2005d Accounting for beta-particle loss to cortical bone vie paired-image radiation transport (PIRT) *Med.Phys.* **32** (5), 1354-1366

Spiers F W 1963 III. Interim Report on the determination of dose to bone marrow from radiological procedures *Br.J.Radiol.* **36**, No 424, 238-240

Spiers F W 1969 Transition-Zone Dosimetry *Radiation Dosimetry* Second Edition, Volume III, Sources, Fiels, Measurements and Applications, Academic Press, New York and London

Spiers F W 1974 Radionuclides and bone – from $^{226}$Ra to $^{90}$Sr *Br.J.Radiol.* **47**, No 564, 833-844

Spiers F W, Beddoe A H and Whitwell J R 1978 Mean skeletal dose factors for beta-particle emitters in human bone. Part I: volume-seeking radionuclides *Br.J.Radiol.* **51**, No. 608, 622-627

Spiers F W, Whitwell and Beddoe A H 1978 Calculated Dose Factors for the Radiosensitive Tissues in Bone Irradiated by Surface-deposited Radionuclides *Phys.Med.Biol.* **23**, No. 3, 481-494

Spiers F W, Beddoe A H and Whitwell J R 1981 Mean skeletal dose factors for beta-particle emitters in human bone. Part I: surface-seeking radionuclides *Br.J.Radiol.* **54**, No. 642, 500-504

Spiers F W 1988 Particle dosimetry in bone and the toxicity of bone-seeking radionuclides *Phys.Med.Biol.* **33**, No. 4, 395-411

Stabin M G, Eckerman K F, Bolch W E, Bouchet L G and Patton P W 2002 Evolution and Status of Bone and Marrow Dose Models *Canc.Bioth.Radiopharm.* **17**, No. 4, 427-433

Whitwell J R and Spiers F W 1976 Calculated Beta-ray Dose Factors for Trabecular Bone *Phys.Med.Biol.* **21**, No. 1, 16-38

Xu X G, Chao T C and Bozkurt A 2000 VIP-MAN: An Image-based Whole-body Adult Male Model Constructed From Colour Photographs Of The Visible Human Project For Multi-particle Monte Carlo Calculations *Health Phys.* **78**(5):476-486

Zankl M, Drexler G, Petoussi-Henss N, Saito K 1997 The Calculation of Dose from External Photon Exposures Using Reference Human Phantoms and Monte Carlo Methods. Part VII: Organ Doses due to Parallel and Environmental Exposure Geometries. *GSF-Report 8/97*. Institut für Strahlenschutz, GSF-Forschungszentrum für Umwelt und Gesundheit, Neuherberg-Muenchen

Zankl M and Wittmann A 2001 The adult male voxel model GOLEM segmented from whole-body CT patient data, *Radiat Environ Biophys*, **40**: 153-162

Zankl M, Petoussi-Henss N, Fill U and Regulla D 2002 Tomographic anthropomorphic models. Part IV: Organ doses for adults due to idealized external photon exposures, GSF – National Research Center for Environment and Health, Neuherberg, Germany, *GSF-Report 13/02*